

Polyoxometalate macroion induced phase and morphology instability of lipid membrane†

Cite this: *Chem. Sci.*, 2013, **4**, 3818

Benxin Jing,^a Marie Hutin,^c Erin Connor,^a Leroy Cronin^{*c} and Yingxi Zhu^{*ab}

The interaction of multivalent macroions with cell membrane can have a profound and significant impact on the functionality and viability of the cell membrane, and this is also critically related to drug and gene delivery as well as nanomaterial cytotoxicity. Using AFM, calorimetry, and light scattering techniques, we have investigated the effect of an anionic polyoxometalate (POM) nanocluster as a model macroion on the phase and structural stability of a lipid bilayer. A POM is distinct from commonly used nanoparticles, in this case comprising a stoichiometric and ordered crystalline nanocluster of typically <5 nm in dimension with uniformly distributed high surface charge density. We have found that the anionic POM nanocluster can strongly adsorb onto a zwitterionic lipid bilayer, which is usually considered as neutral and uncharged, due to the strong electrostatic attraction in a similar fashion to the interaction of a POM with a cationic lipid bilayer. More interestingly, the adsorption of POM also results in the gelation of the lipid bilayer that is otherwise in the fluid phase in the absence of the POM macroion. By examining lipid bilayers with varied lipid headgroup chemistry and phase state, we have revealed that the energy released upon the POM adsorption on the lipid bilayer is contributed not only from the enthalpy associated with gelation, but also from the entropy associated with local surface reconstruction of the lipid bilayer. A POM-induced entropic penalty on the lipid bilayer is confirmed by both liposome shrinkage and bilayer morphological disruption, including the formation of pores, buds, and multilayer stacks on a POM-adsorbed lipid membrane. Hence, the accompanied phase and morphological instability induced by the POM is unique and surprising, in contrast to the fact that only one, but not both, of the phenomena has been reported previously with hydrophilic or hydrophobic nanoparticles. Our results offer an unprecedented new insight into nanomaterial design and selection for controlled molecular transport through cell membranes.

Received 20th May 2013

Accepted 10th July 2013

DOI: 10.1039/c3sc51404h

www.rsc.org/chemicalscience

Introduction

The interaction of macroions, including polyelectrolytes, DNAs, proteins, and highly charged nanocolloids, with lipid membranes is critical to control and ensure selective transport across cell membranes for drug and gene delivery as well as protecting cells against the environment.^{1–4} Multivalent macroions can significantly alter the local composition and morphology of cell membranes upon adsorption and translocation, which raises the concern of their biocompatibility and cytotoxicity.^{5–9} Much of the prior work on the macroion interaction with lipid membranes has mainly focused on charged

nanoparticles or polyelectrolytes including dendrimers,^{10,11} synthetic polycations,¹² DNA,^{2,13} peptides,^{3,14,15} and proteins.^{6,16,17} However, it is nearly impossible to accurately locate the charges on these macroions in that the charges on these nanocolloidal or macromolecular surfaces are often inhomogeneously distributed and can be largely altered by local ionic environment or their own conformational change upon the translocation through lipid membranes, thus their interaction with biomembranes remains poorly understood. Furthermore, the size of the macroions could also complicate the matter, especially when the size of the macroions becomes comparable to that of the lipid molecules and lipid bilayers. In the size range of 1–10 nm, it is difficult to precisely estimate the electrostatic interaction between macroions and lipid bilayer because the macroions could not be simply treated as a point charge; yet to date, it remains a grand challenge to solve the non-linear Poisson–Boltzman equation for macroion–biomembrane interaction while the Debye–Hückel approximation becomes invalid for the macroion case. To simplify this case and make it possible to understand the electrostatic interaction of macroions with biomembranes, one ideal macroion case is a

^aDepartment of Chemical and Biomolecular Engineering, University of Notre Dame, Notre Dame, Indiana 46556, USA. E-mail: yzhu3@nd.edu; Fax: +1 574-631-8366; Tel: +1 574-631-2667

^bDepartment of Chemistry and Biochemistry, University of Notre Dame, Notre Dame, Indiana 46556, USA

^cSchool of Chemistry, University of Glasgow, Glasgow G12 8QQ, UK. E-mail: L.Cronin@chem.gla.ac.uk; Fax: +44 (0)141 330 4888; Tel: +44 (0)141 330 6650

† Electronic supplementary information (ESI) available. See DOI: 10.1039/c3sc51404h

hydrophilic macroion of radius, $R < 5$ nm with well-defined and fixed surface structure and charge distribution, in which the long-debated hydrophobic interaction can be also neglected. In this work, we select a novel model macroion, which features stoichiometric and ordered crystalline nanocluster structure and extremely high yet stable surface charge density, to study its interaction with a lipid bilayer that is considered as a model cell membrane.

The model macroion selected in this work is based upon an anionic POM. POMs are the assemblies of transition metal oxides $\{MO_x\}$ where $x = 4-7$ and M is generally Mo, W, V, U and Nb forming clusters with well-defined atomic coordination structure and typically 1–5 nm in size. They have recently emerged as novel functional nanomaterials^{18–25} used for catalysis,^{26,27} semiconductors,²⁸ anti-cancer and anti-virus treatment,^{29–32} thanks to their unique chemical, optical and electrical characteristics. Importantly, it should be noted that POMs are fundamentally different from nanocolloids because they can dissolve into polar solvents to form thermodynamically stable solutions, sharply distinct from colloidal suspensions formed by nanoparticles in liquids.³³ It has recently been reported that POMs could insert and translocate across cell membranes for anti-cancer treatment,^{29,34} yet their interaction with cell membranes as related to their implication in cytotoxicity and drug delivery remains poorly understood. Previous work performed with large colloidal macroions suggests that semi-hydrophobic and some hydrophilic nanoparticles could induce the morphological disruption of a lipid membrane while other hydrophilic nanoparticles could cause the phase transition of the lipid bilayer, yet no consensus or fundamental understanding has been achieved due to the size and surface complexity of nanoparticles. Considering the compatible size of POM nanoclusters with the lipid bilayer and its well-defined surface charges, as well as their strong hydrophilicity and high solution stability, POMs at lipid bilayer interfaces open a new avenue to examine and understand the interaction between macroions and cell membranes. The observations and then the analysis of the POM-induced phenomena by using combined AFM, light scattering, and calorimetry methods are therefore particularly relevant for a better understanding of the biological processes at the macroion–biomembrane interfaces.

Specifically, the macroion selected in this work is the wheel-like $[(MoO_3)_{176}(H_2O)_{80}]Na_{32}$ nanocluster ($\{Mo_{176}\}$) of 4.10 nm in diameter and 1.35 nm in thickness (Fig. 1a).^{35,36} The net 32 negative charges are uniformly distributed, yielding a surface charge density of $\sim 1 e^- nm^{-2}$, which is at least 5-fold higher than that of charged polymer-functionalized latex or silica nanoparticles at this size range. However, it should be noted that the surface charge density of $\{Mo_{176}\}$ macroion is not high enough for counterion condensation because the separation distance between two adjacent charges is ~ 1 nm and higher than the Bjerrum length.³⁷ In this work, we have observed that $\{Mo_{176}\}$ can strongly adsorb on a zwitterionic lipid bilayer that is commonly treated as uncharged or net neutral and subsequently cause the surface patchiness and gelation in a lipid bilayer that is otherwise in the fluid phase. POM-induced

gelation of a zwitterionic lipid bilayer is new and has not been previously observed with charged hydrophilic nanoparticles of $R < 10$ nm or polyelectrolytes including DNAs and peptides. To assess the generality of this POM-induced phase and morphological change in lipid bilayer, a similar study has been conducted using an $\{Se_{16}W_{101}\}$ POM macroion, which is structurally and chemically different from $\{Mo_{176}\}$ and carries 52 negative charges over an averaged radius of $R = 1.60$ nm with a resultant effective surface charge density of $\sim 1.6 e^- nm^{-2}$. Similar results have been obtained as detailed in the ESI (see Fig. S1–S3†).

Experimental section

Lipids and lipid bilayer preparation

α -PC (1- α -phosphatidylcholine), DOTAP (1,2-dioleoyl-3-trimethylammonium-propane (chloride salt)), DC₁₅PC (1,2-dipentadecanoyl-*sn*-glycero-3-phosphocholine), DOPA (1,2-dioleoyl-*sn*-glycero-3-phosphate (sodium salt)), and DSPC (1,2-distearoyl-*sn*-glycero-3-phosphocholine) lipids, whose molecular structures are depicted in Fig. 1a, are all obtained from Avanti Polar Lipids and used directly. Small unilamellar vesicles (SUVs) of lipids are prepared with $5.0 g L^{-1}$ lipids (~ 60 nM liposomes) in 0.02 M sodium acetate/acetic acid buffer (pH 3.80, which is among the normal pH range in a human stomach³⁸) by sonication in a bath sonicator (Model G112SPIG, Laboratory Supplies) for 30 min. The hydrodynamic radius, R_H , and zeta potential, ζ , of liposomes are measured by a Zeta Potential Analyzer (ZetaPlus, Brookhaven Instruments) at the University of Notre Dame. Single crystal silicon wafers with one side polished (Silicon Quest International) are cleaned in a heated piranha solution (30% H₂O₂ and 70% H₂SO₄) at $T = 120$ °C for 1 h before experiment. Supported lipid bilayers (SLBs) are prepared by rupturing and spreading liposomes on a cleaned silicon wafer and excess SUVs are rinsed away by acetate buffer solution.

$\{Mo_{176}\}$ nanocluster synthesis

The synthesis of $[(MoO_3)_{176}(H_2O)_{80}]Na_{32}$ is conducted at the University of Glasgow by following the published procedure except using Na₂MoO₄ instead of Li₂MoO₄.³⁶ In this work, $\{Mo_{176}\}$ is dissolved in acetate buffer at a concentration range of 10 nM to 51.0 μ M, and used immediately after being well mixed (*via* shaking for several minutes). It should be noted that no decomposition of the $\{Mo_{176}\}$ nanocluster is observed during the first 6 hours at 25 °C and 60 °C after the preparation of $\{Mo_{176}\}$ solution (see Fig. S4 in ESI†), which indicates the high chemical stability of $\{Mo_{176}\}$ in aqueous solution in the time window of this work. More importantly, no “blackberry”-like $\{Mo_{176}\}$ assembly as reported in other similar Mo-based POM nanoclusters^{22,25,33} is observed in the $\{Mo_{176}\}$ solution even after a storage period of ~ 1 year as confirmed by dynamic light scattering, small angle X-ray (SAXS), and UV-vis spectroscopy measurements (see Fig. S4 in ESI†), indicating the high dispersion stability of the $\{Mo_{176}\}$ macroion.

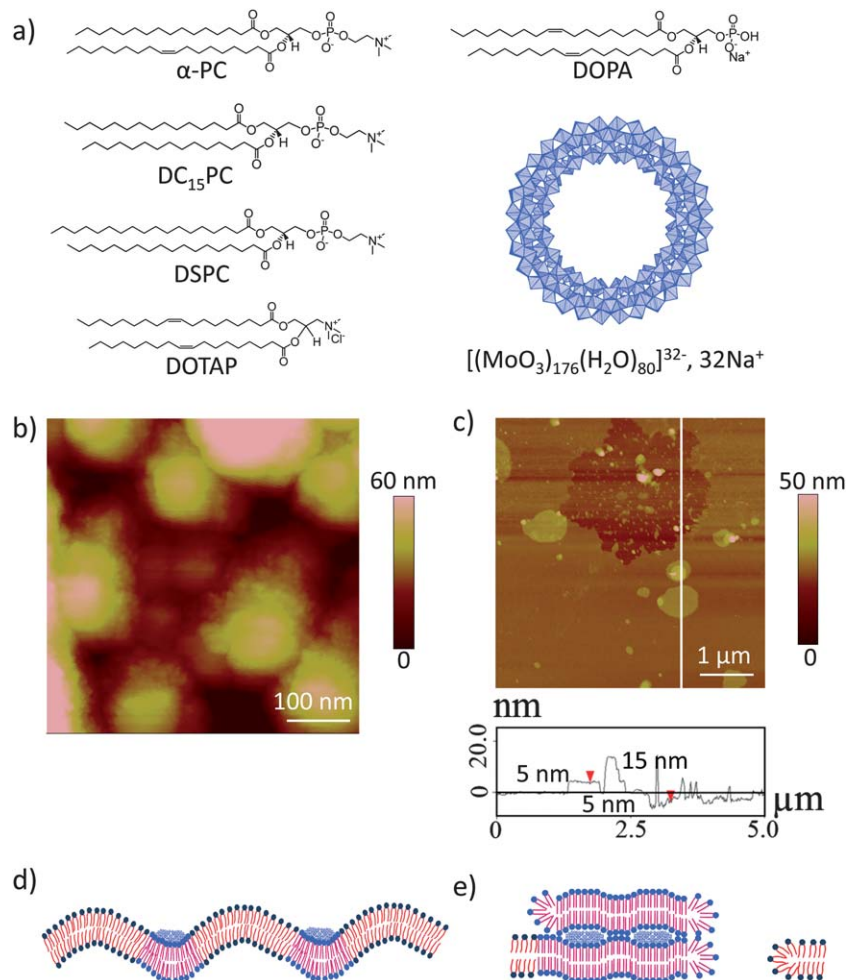


Fig. 1 (a) Chemical structure of lipids and $\{Mo_{176}\}$ macroion used in this work. (b) AFM micrograph showing the morphological structure of α -PC liposomes added with $\{Mo_{176}\}$ at a molar ratio of $\{Mo_{176}\}$ to α -PC lipid about 0.013 in 0.02 M NaAc-HAc buffer (pH 3.80), corresponding to the schematic illustration in (d). (c) AFM micrograph showing the morphological structure of a supported α -PC bilayer on a clean silicon wafer with added 8.42 μ M $\{Mo_{176}\}$ and 0.02 M NaAc-HAc buffer (pH 3.80), corresponding to the schematic illustration in (e). Section analysis along the white line shows the height profile of the $\{Mo_{176}\}$ -adsorbed supported α -PC bilayer.

Characterization

Calorimetric experiments are conducted with isothermal titration calorimetry (GE Microcal Isothermal Titration Calorimeter, iTC₂₀₀) at the University of Notre Dame. Typically, 26 consecutive aliquots of 1.5 μ L each for $\{Mo_{176}\}$ at a concentration of 2.0 g L⁻¹ are injected into a 200 μ L liquid cell filled with 0.25 g L⁻¹ liposome solution. Subsequent injection of $\{Mo_{176}\}$ is made at a time intervals of 200 s and a rate of 0.75 μ L s⁻¹. A constant stirring speed of 1000 rpm is maintained throughout the experiment to ensure sufficient mixing after each injection. To calculate the binding isotherm, the heat of dilution is calibrated with separate $\{Mo_{176}\}$ buffer titrations for the baseline subtraction. "One Set of Sites Model" is used to fit the results.³⁹

The morphological structure of supported lipid bilayers (SLBs) and liposomes on a silicon wafer in acetate buffer is characterized by an AFM operated in the tapping mode (Multimode, Nanoscope IV Controller, Veeco) with a silicon nitride probe (NP, Veeco) and water-proof scanner (J scanner, Veeco) at room temperature. The tapping-mode fluid cell (MTFML, Veeco) with O-ring is cleaned with copious ethanol

and blow-dried in a stream of nitrogen. To get a high quality image, the resonance frequency of the AFM probe in aqueous solution is fixed between 9 kHz and 10 kHz.

Results and discussion

Initially we start with tapping-mode AFM to examine the morphological structure of the zwitterionic α -PC bilayer in both SUV and SLB in $\{Mo_{176}\}$ -added acetate buffer solution (pH = 3.80). It is noted that in the buffer solutions without added $\{Mo_{176}\}$, a homogeneous and featureless α -PC SLB is observed (see Fig. S2a in ESI†). It is expected that no liposomes will be observed by AFM because they are so fluid and mobile that they can be readily ruptured and spread on the highly hydrophilic silicon surface upon adsorption to form a homogeneous SLB and the attraction between the liposome and SLB is very weak. Surprisingly, liposomes with corrugated surfaces can be clearly observed by AFM immediately after adding $\{Mo_{176}\}$ (Fig. 1b), indicating elevated rigidity and roughness of the liposomes due to adsorbed $\{Mo_{176}\}$. Additionally, the roughened liposome surface exhibits many buds of >10 nm in the lateral dimension

and 0.5–1.5 nm in the direction normal to the liposome surface, suggesting the bending of the lipid membrane with embedded $\{\text{Mo}_{176}\}$ due to a strong attraction between $\{\text{Mo}_{176}\}$ and α -PC lipids as schematically illustrated in Fig. 1d. $\{\text{Mo}_{176}\}$ -induced morphological change is also observed with α -PC SLB with the presence of pores and multilayer patches (Fig. 1c): the depth of the pores is nearly the same with the thickness of SLB while the thickness of multilayer patches is integer multiples of the thickness of one lipid bilayer. This suggests that the stacking of lipid bilayers are dragged from the original regions where $\{\text{Mo}_{176}\}$ -induced pores are formed, as schematically illustrated in Fig. 1e. Such morphological disruption has not been previously observed with any other macroions adsorbed on a lipid bilayer^{4,9–12,15,40–42} and is possibly a result of the significantly strong attraction between $\{\text{Mo}_{176}\}$ and α -PC. Considering the strong $\{\text{Mo}_{176}\}$ -lipid attraction, we expect that the dragging of lipid molecules from α -PC SLB by the adsorbed anionic $\{\text{Mo}_{176}\}$ nanocluster is energetically favoured, which subsequently results in the observed lipid multilayer stacking (Fig. 1c).

Based on the observations above and the fact that $\{\text{Mo}_{176}\}$ is anionic and α -PC is zwitterionic, we believe the strong attraction between hydrophilic $\{\text{Mo}_{176}\}$ and α -PC bilayer should be of electrostatic origin and associated with the positively charged choline in the zwitterionic head group of α -PC lipid facing closer towards $\{\text{Mo}_{176}\}$ than the negatively charged phosphate. We have approximately estimated the $\{\text{Mo}_{176}\}$ - α -PC bilayer interaction by depicting the nanocluster as a charged ring, whose net charge of $Q = 32 e^-$ is uniformly smeared over its wheel-like rim of radius, $R_{\{\text{Mo}_{176}\}} = 2.05$ nm and angle, $\phi' = [0, 2\pi]$ on the “membrane-apposed” plane. Since counterion condensation could be neglected for $\{\text{Mo}_{176}\}$ in aqueous solution, not any charge on $\{\text{Mo}_{176}\}$ is neutralized by counterions in solution. Thus, the electric potential, $V(r, \phi, z)$, generated by $\{\text{Mo}_{176}\}$ in a cylindrical coordination (as schematically defined in Fig. S5a in ESI†) can be approximately expressed as:⁴³

$V(r, \phi, z) =$

$$\frac{1}{4\pi\epsilon\epsilon_0} \frac{Q}{2\pi} \int_0^{2\pi} \frac{d\phi'}{\sqrt{r^2 - 2rR_{\{\text{Mo}_{176}\}}\cos(\phi - \phi') + R_{\{\text{Mo}_{176}\}}^2 + z^2}}, \quad (1)$$

where $\epsilon\epsilon_0$ is the permittivity of water. As α -PC lipid headgroup is simplified as one dipole, due to its zwitterionic nature, with a length of $l = 0.63$ nm and a tilting angle of 25° relative to the normal to the membrane plane based on chemical structure measurements.⁴⁴ The electrostatic pair interaction energy, $E_{\text{potential}}$, between a $\{\text{Mo}_{176}\}$ and α -PC lipid bilayer can be estimated as

where $\rho_e (=0.55$ lipids per $\text{nm}^2)$ is the surface density of lipid molecules in SLB, r_0 is the radius of the α -PC lipid bilayer plane. Considering sufficiently high coverage of $\{\text{Mo}_{176}\}$ on lipid bilayer and electrostatic screening effect, we reasonably assume that one $\{\text{Mo}_{176}\}$ can only interact with lipids on its projected lipid bilayer region, but not with the far-reaching lipids, the latter of which might cause a slight underestimation of the $\{\text{Mo}_{176}\}$ -lipid interaction. According to eqn (2) for the pair interaction between a $\{\text{Mo}_{176}\}$ of $R_{\{\text{Mo}_{176}\}} = 2.05$ nm and an α -PC bilayer of $r_0 = 2.05$ nm, $E_{\text{potential}}$ is computed by MATLAB. It is found that $E_{\text{potential}}$ can drastically change from $-6k_B T$ to $-30k_B T$ when the closest distance between $\{\text{Mo}_{176}\}$ and the lipid bilayer decreases from $z = 6$ nm, that is approximate to the electric screening length, to $z = 1.35$ nm, that corresponds to the measured $\{\text{Mo}_{176}\}$ thickness from the crystal structure data, respectively. Despite its strong dependence on z , the electrostatic attraction between $\{\text{Mo}_{176}\}$ and lipid bilayer is considerably strong, allowing the adsorption of $\{\text{Mo}_{176}\}$ on the net neutral lipid bilayer. In a similar approach to calculate the interaction between $\{\text{Mo}_{176}\}$ and positively-charged phospholipid, we have found that the estimated electrostatic attraction of $\{\text{Mo}_{176}\}$ with zwitterionic α -PC lipid bilayer is weaker than that with cationic lipid by only a factor of 7–14 that depends on z (Fig. S5b in ESI†). It is strongly indicated that the anionic $\{\text{Mo}_{176}\}$ macroion can be strongly adsorbed on the zwitterionic lipid bilayer similar to the adsorption on an oppositely charged bilayer.

The strong attraction between $\{\text{Mo}_{176}\}$ and α -PC lipid is also evidently inferred from the excellent solubility of $\{\text{Mo}_{176}\}$ and α -PC mixture in chloroform, in which hydrophilic $\{\text{Mo}_{176}\}$ could not be dissolved alone (Fig. S6 in ESI†). We observe that $\{\text{Mo}_{176}\}$ readily transfers from the aqueous phase to the α -PC lipid-added chloroform phase with a resulting colour change in the chloroform solution, in contrast to no colour change in lipid-free chloroform solution, which strongly suggests the formation of $\{\text{Mo}_{176}\}$ and α -PC complex in chloroform similar to the complex formation between cationic surfactants and POMs.^{45,46}

In addition, the strong electrostatic attraction can even lead to a deformation of the lipid membrane by $\{\text{Mo}_{176}\}$ (Fig. 1d), which agrees with a previous prediction for macroions on a charged lipid bilayer.⁸ We estimate the resulting curvature radius, R_B , of the lipid bilayer after spherical bending upon $\{\text{Mo}_{176}\}$ adsorption to be about 4.2 nm by approximating the bending energy, E_{bend} to $|E_{\text{potential}}| \approx 30k_B T$ at the closest $\{\text{Mo}_{176}\}$ -lipid separation distance of $z = 1.35$ nm and using eqn (3),⁴⁷

$$E_{\text{potential}} = \frac{\rho_e}{4\pi\epsilon\epsilon_0} \frac{Q}{2\pi} \int_0^{2\pi} \int_0^{r_0} \int_0^{2\pi} \left(\frac{1}{\sqrt{r^2 - 2rR_{\{\text{Mo}_{176}\}}\cos(\phi - \phi') + R_{\{\text{Mo}_{176}\}}^2 + z^2}} - \frac{1}{\sqrt{r^2 - 2rR_{\{\text{Mo}_{176}\}}\cos(\phi - \phi') + R_{\{\text{Mo}_{176}\}}^2 + (z + l \cos 25^\circ)^2}} \right) r d\phi dr d\phi', \quad (2)$$

$$E_{\text{bend}} = \frac{2k_c A}{R_B^2}, \quad (3)$$

where $A (= \pi r_0^2)$ is the interacting area of lipid bilayer, and k_c is the bending modulus of the lipid bilayer and is roughly $20.7k_B T$ based on the reported value for POPC lipid, the major composition of α -PC.⁴⁸ Hence, we obtain the bud height,

$$h = R_B - \sqrt{R_B^2 - r_0^2}, \quad (4)$$

as about 0.5 nm, which is almost consistent with our observation (Fig. 1b and 4c). $\{\text{Mo}_{176}\}$ -induced deformation in the lipid bilayer is also verified by AFM with net anionic liposomes containing 20% anionic DOPA and 80% zwitterionic α -PC, which is a result of the strong attraction between $\{\text{Mo}_{176}\}$ and α -PC.

It should be noted that no supported lipid multilayer patches or buds on the lipid bilayer in a fluid phase have been previously captured by tapping-mode AFM, simply because the lipid bilayer in the fluid phase is very mobile and the AFM tip can easily drag and disrupt it due to the weak attraction between lipid bilayers. Surprisingly, we have demonstrated in our case that $\{\text{Mo}_{176}\}$ macroion-induced morphological disruption on both α -PC liposome and SLB is very stable without any further changes in these already formed pores and multilayer stacks after repeated AFM scanning. The only exception is found with very low $\{\text{Mo}_{176}\}$ concentration (<12.7 nM), in which we indeed

observe the smudging of $\{\text{Mo}_{176}\}$ -induced multilayer stacks after several AFM scanning cycles (Fig. S7 in ESI†), indicating that the lipid bilayer remains very soft and mobile possibly owing to the sufficiently low surface coverage of adsorbed $\{\text{Mo}_{176}\}$. Since this $\{\text{Mo}_{176}\}$ -induced morphological disruption in the lipid bilayer is always concomitantly accompanied by the dramatic suppression of the mobility of individual lipid molecules in lipid bilayer (see Fig. S1b and S7 in ESI†), we surmise that a fluid-to-gel phase transition of the lipid bilayer is also induced by the adsorption of $\{\text{Mo}_{176}\}$ when a critical $\{\text{Mo}_{176}\}$ concentration is exceeded.

To validate this scenario, we have employed isothermal titration calorimetry (ITC) to directly measure the enthalpy change, ΔH , of liposomes upon $\{\text{Mo}_{176}\}$ adsorption (Fig. 2). The heat flow change in the α -PC liposome suspension after adding $\{\text{Mo}_{176}\}$ (Fig. 2a) clearly indicates that the binding of $\{\text{Mo}_{176}\}$ to the α -PC bilayer is an exothermic process, in sharp contrast to the endothermic process for adding $\{\text{Mo}_{176}\}$ to a liposome-free buffer solution (inset of Fig. 2a). It should be noted that the “tail-up” in the initial stage of ITC curves in Fig. 2b possibly resulted from insufficient enthalpy change associated with the increased liposome size and size polydispersity at low $\{\text{Mo}_{176}\}$ concentration (see the discussion of Fig. 3a below). The observed exothermic binding strongly supports our picture of adsorbed $\{\text{Mo}_{176}\}$ -induced gelation of the α -PC lipid bilayer, was consistent with experimental, theoretical and computer

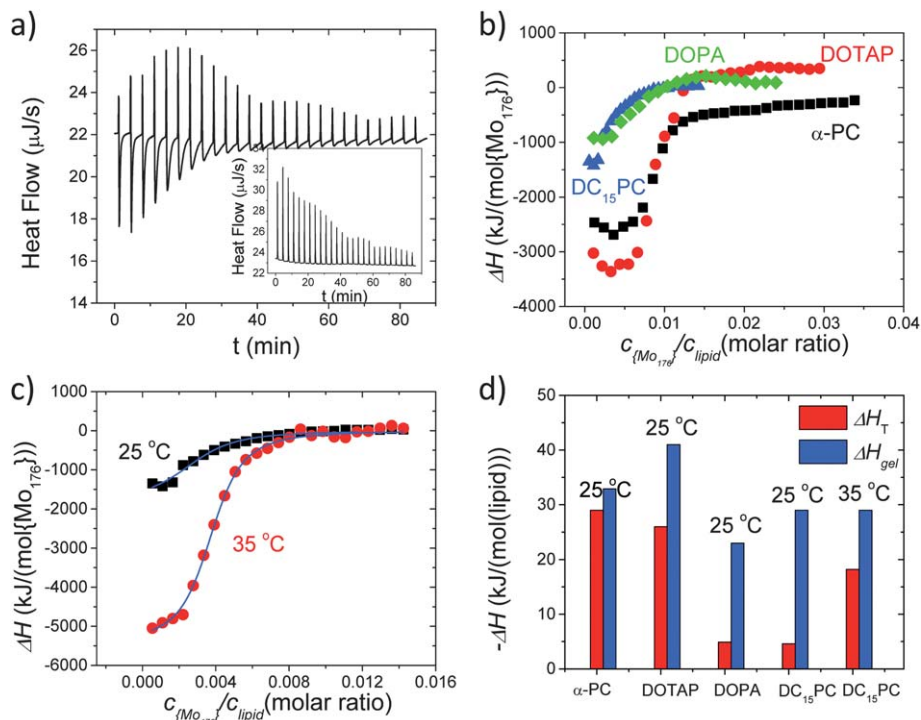


Fig. 2 (a) Heat flow change of α -PC liposome-added buffer suspension after adding $\{\text{Mo}_{176}\}$, as measured by ITC. Inset: heat flow change of liposome-free buffer solution after adding $\{\text{Mo}_{176}\}$. (b) Enthalpy change, ΔH normalized by $\{\text{Mo}_{176}\}$ concentration at $T = 25^\circ\text{C}$, after the subtraction of the heat of dilution, against the molar ratio of $\{\text{Mo}_{176}\}$ to lipid, $c_{\{\text{Mo}_{176}\}}/c_{\text{lipid}}$, for α -PC (black squares, $R_H = 55$ nm), DOTAP (red circles, $R_H = 58$ nm), DOPA (green diamonds, $R_H = 87$ nm), and DC₁₅PC (blue triangles, $R_H = 62$ nm). The fitting yields the binding constant, K_a as summarized in Table 1. (c) Enthalpy change, ΔH , per $\{\text{Mo}_{176}\}$ in DC₁₅PC liposome suspensions against $c_{\{\text{Mo}_{176}\}}/c_{\text{lipid}}$ at $T = 25^\circ\text{C}$ (black squares), at which DC₁₅PC is in a gel phase, and $T = 35^\circ\text{C}$, at which DC₁₅PC is in a fluid phase. (d) The comparison of total enthalpy change per lipid after adding $\{\text{Mo}_{176}\}$, ΔH_T , to their reported fluid-to-gel phase transition enthalpy change, ΔH_{gel} .

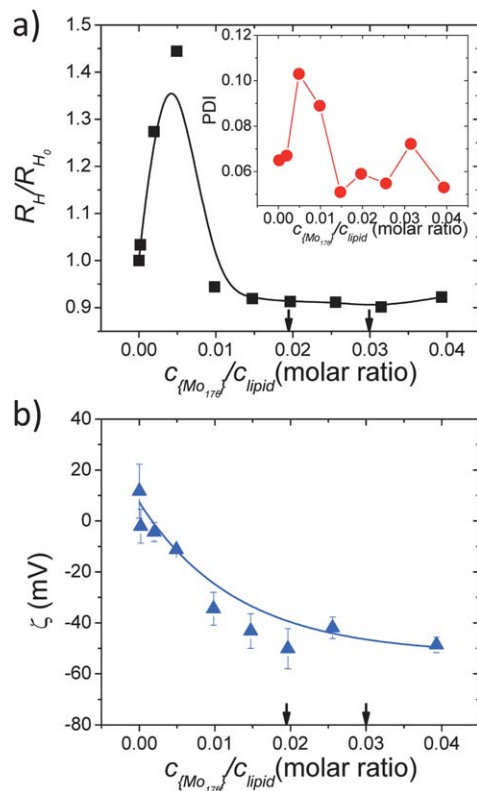


Fig. 3 (a) The ratio of measured α -PC liposome radius after adding $\{\text{Mo}_{176}\}$ to the original one of bare liposomes against $c_{\{\text{Mo}_{176}\}}/c_{\text{lipid}}$ at $T = 25^\circ\text{C}$. Inset: polydispersity in the measured $\{\text{Mo}_{176}\}$ -dressed liposome size against $c_{\{\text{Mo}_{176}\}}/c_{\text{lipid}}$. (b) Zeta potential, ζ of α -PC liposome after adding $\{\text{Mo}_{176}\}$ against $c_{\{\text{Mo}_{176}\}}/c_{\text{lipid}}$ at $T = 25^\circ\text{C}$.

simulation observations of anionic nanoparticles of $R \geq 10$ nm inducing the fluid-to-gel phase transition in zwitterionic lipid bilayers.^{4,7,41} The integration of ΔH normalized by $\{\text{Mo}_{176}\}$ concentration (Fig. 2b) yields the total enthalpy change, ΔH_T , which in this process is $358k_B T$ per $\{\text{Mo}_{176}\}$. Because the size of $\{\text{Mo}_{176}\}$ is much smaller than the commonly used charged nanoparticles ($R \geq 10$ nm), the critical molar ratio of $\{\text{Mo}_{176}\}$ to lipid for the onset of gelation is about ten-fold greater than that of nanoparticles on similar biomembranes yet the obtained ΔH_T on a similar lipid bilayer is comparable between the two cases.⁴ Furthermore, the curve fitting yields the binding constant of $\{\text{Mo}_{176}\}$ on the α -PC liposome to be $K_a \sim 6.5 \times 10^6 \text{ M}^{-1}$, indicating a free energy change,³⁹ $\Delta G = -RT \ln K_a \approx -15.7k_B T$ per $\{\text{Mo}_{176}\}$. The drastic difference between ΔH_T and ΔG clearly reveals a huge *entropic penalty* that mostly arises from the loss of entropy in the gelled lipids as further discussed below.

To examine the generality of $\{\text{Mo}_{176}\}$ -induced gelation of lipid bilayers, we have compared the enthalpy change in different liposomes of varied lipid headgroup chemistry and lipid phase transition temperature. In addition to zwitterionic α -PC whose phase transition temperature, T_{gel} , is approximately -2.6°C , similar ITC experiments are also conducted with cationic DOTAP ($T_{\text{gel}} = -11.9^\circ\text{C}$), anionic DOPA ($T_{\text{gel}} = -8^\circ\text{C}$), and zwitterionic (DC₁₅PC) ($T_{\text{gel}} = 33^\circ\text{C}$) (Fig. 2b). The fitting of measured ΔH versus $c_{\{\text{Mo}_{176}\}}/c_{\text{lipid}}$ yields the corresponding K_a

Table 1 The fluid-to-gel transition temperature, T_{gel} , and enthalpy change upon the phase transition, ΔH_{gel} reported in the literature, measured binding constant and free energy change of varied lipids with adsorbed $\{\text{Mo}_{176}\}$ in this work

Lipids	T_{gel}^a ($^\circ\text{C}$)	ΔH_{gel}^a (kJ mol^{-1})	K_a ($\times 10^6 \text{ M}^{-1}$)	ΔG ($k_B T$ per $\{\text{Mo}_{176}\}$)
α -PC	-2.6	-32.9	6.5	-15.7
DC ₁₅ PC (gel)	33	-29.0	2.3	-14.6
DC ₁₅ PC (fluid)	—	—	7.6 ^b	-15.8 ^b
DSPC	55	-38.0	—	—
DOTAP	-11.9	-41.0	37	-17.4
DOPA	-8	-23.0	15	-16.5

^a The phase transition temperature, T_{gel} , and enthalpy change, ΔH_{gel} of varied lipids in this table are obtained from ref. 13 and 49–52. The data of α -PC are obtained from its major composition, 1-palmitoyl-2-oleoyl-*sn*-glycero-3-phosphocholine (POPC). ^b The free energy data here is obtained at 35°C . All other binding free energy data are obtained at 25°C .

and ΔG for different lipids as summarized in Table 1. As the integrated ΔH_T per lipid concentration for different lipids is summarized in Fig. 2d, the ΔH_T upon $\{\text{Mo}_{176}\}$ adsorption exhibits a strong dependence on the lipid headgroup chemistry and phase state. The interaction and resulting ΔH_T of cationic DOTAP with $\{\text{Mo}_{176}\}$ exhibits a very similar behaviour to α -PC liposomes and much stronger than that for anionic DOPA in the fluid phase and zwitterionic DC₁₅PC in the gel phase at $T = 25^\circ\text{C}$. This trend confirms that a strong electrostatic attraction is the dominant driving force for the adsorption of anionic $\{\text{Mo}_{176}\}$ on zwitterionic and cationic lipid bilayers, causing subsequent bending and gelation of the lipid bilayer at the positions where $\{\text{Mo}_{176}\}$ adsorbs. Furthermore, as we compare the difference of $\{\text{Mo}_{176}\}$ -induced ΔH_T of DC₁₅PC liposome between the gel and fluid phases (Fig. 2c), it is intriguing to observe that the measured $\Delta H_T = 325k_B T$ per $\{\text{Mo}_{176}\}$ of DC₁₅PC liposomes in the fluid phase at $T = 35^\circ\text{C}$ is much higher than $\Delta H_T = 95k_B T$ per $\{\text{Mo}_{176}\}$ in the gel phase at $T = 25^\circ\text{C}$. Considering that the only difference here is their phase state, or their lipid packing density and configuration while the interaction between $\{\text{Mo}_{176}\}$ and DC₁₅PC headgroup remains nearly the same, we contribute this huge difference to be equivalent to the resulting enthalpy release from adsorbed $\{\text{Mo}_{176}\}$ -induced gelation of the DC₁₅PC bilayer in the original fluid phase. According to the reported fluid-to-gel transition enthalpy,^{13,49–52} the ratio of measured ΔH_T to their corresponding ΔH_{gel} is 0.88 for α -PC, 0.63 for DOTAP, and 0.63 for DC₁₅PC in the fluid phase in contrast to the ratio of 0.16 for DC₁₅PC in the gel phase (Fig. 2d), clearly indicating the dominant contribution of $\{\text{Mo}_{176}\}$ -induced gelation in the fluid lipid bilayer to the measured enthalpy release.

To investigate the concomitant morphological change of the lipid bilayer with $\{\text{Mo}_{176}\}$ -induced gelation, we examine the change in R_H and ζ of α -PC liposomes against $\{\text{Mo}_{176}\}$ concentration (Fig. 3a and b). At a low $\{\text{Mo}_{176}\}$ -to- α -PC lipid molar ratio, $c_{\{\text{Mo}_{176}\}}/c_{\text{lipid}} < 0.01$, the size of α -PC liposomes increases rapidly with increasing $\{\text{Mo}_{176}\}$, suggesting $\{\text{Mo}_{176}\}$ macroion-mediated bridging across liposomes to form $\{\text{Mo}_{176}\}$ -liposome aggregates, also leading to the considerable increase of liposome size

polydispersity (inset of Fig. 3a) and the eventual precipitation of some $\{\text{Mo}_{176}\}$ -liposome aggregates from an aqueous suspension. In contrast, at $c_{\{\text{Mo}_{176}\}}/c_{\text{lipid}} > 0.01$, the measured radius of α -PC liposome appears to monotonically decrease from its original size of 55 nm to 50 nm, resulting in a 17% increase in lipid surface packing density, closely approximate to the predicted increase of 25% upon a fluid-to-gel phase transition.⁵³ Also, due to the high charge density of the $\{\text{Mo}_{176}\}$ macroion,

the colloidal stability of $\{\text{Mo}_{176}\}$ -dressed liposomes is significantly enhanced without noticeable liposome fusion over a time period longer than 25 days, over which further size shrinkage is conversely observed (Fig. S8 in ESI†). Accompanied by the decrease of liposome size is the monotonic increase in liposome surface charge negativity as exhibited by measured ζ , further confirming the strong adsorption and resulting high surface coverage of $\{\text{Mo}_{176}\}$ macroions on the liposome surface. Considering that the occupied unit area of a lipid headgroup on the lipid bilayer is $\sim 0.5\text{--}0.8\text{ nm}^2$,⁵³ we estimate that the full coverage of the $\{\text{Mo}_{176}\}$ macroion on a liposome surface can be achieved at $c_{\{\text{Mo}_{176}\}}/c_{\text{lipid}} \sim 0.019\text{--}0.03$ as indicated by the two arrows in Fig. 3a and b. However, this critical molar ratio is much higher than the onset of the plateau region in both Fig. 3a and b, possibly due to the steric effect arising from the strong repulsion between adsorbed $\{\text{Mo}_{176}\}$ macroions and those free ones in the bulk solution.

To verify the general behaviour exhibited in Fig. 3 as well as to further understand the entropic contribution to the measured ΔG of liposomes upon $\{\text{Mo}_{176}\}$ adsorption, we have also compared the change in the size and ζ of zwitterionic DSPC ($T_{\text{gel}} = 55\text{ }^\circ\text{C}$) liposome in its fluid and gel phases. To work within the optimal temperature range of dynamic light scattering and thereby minimize experimental errors, this study has been performed with the DSPC liposome, not the structurally similar DC_{15}PC , simply because of the much better experimental stability and reproducibility for DSPC at varied temperatures across its T_{gel} than that of DC_{15}PC whose T_{gel} is so close to the room temperature as to cause experimental noise. As shown in Fig. 4, the size of the DSPC liposome in the gel phase at $T = 25\text{ }^\circ\text{C}$ remains nearly constant after adding $\{\text{Mo}_{176}\}$, yet at $T = 60\text{ }^\circ\text{C}$ both size and ζ potential of DSPC in the fluid phase change largely with increasing $\{\text{Mo}_{176}\}$ in a similar fashion to $\{\text{Mo}_{176}\}$ -added α -PC liposomes. More interestingly, at $c_{\{\text{Mo}_{176}\}}/c_{\text{lipid}} > 0.01$, DSPC liposome size becomes even smaller when the liposome returns to its gel phase by cooling the mixed suspension back to $T = 25\text{ }^\circ\text{C}$ than that at $T = 25\text{ }^\circ\text{C}$ before heating, further confirming that the shrinkage of the $\{\text{Mo}_{176}\}$ -dressed liposome accompanies the induced gelation. Similar bud formation on DSPC liposomes in the gel phase is also observed (Fig. 4c), further supporting the picture $\{\text{Mo}_{176}\}$ -induced deformation in zwitterionic lipid bilayer upon adsorption. However, the measured ζ potential after cooling back to $T = 25\text{ }^\circ\text{C}$ from $60\text{ }^\circ\text{C}$ is intermediate between the original values before and after heating without exhibiting any correlation with liposome size or surface area change, suggesting that some of $\{\text{Mo}_{176}\}$ macroions can be partially engulfed by the lipid bilayer upon liposome shrinkage during the cooling process.

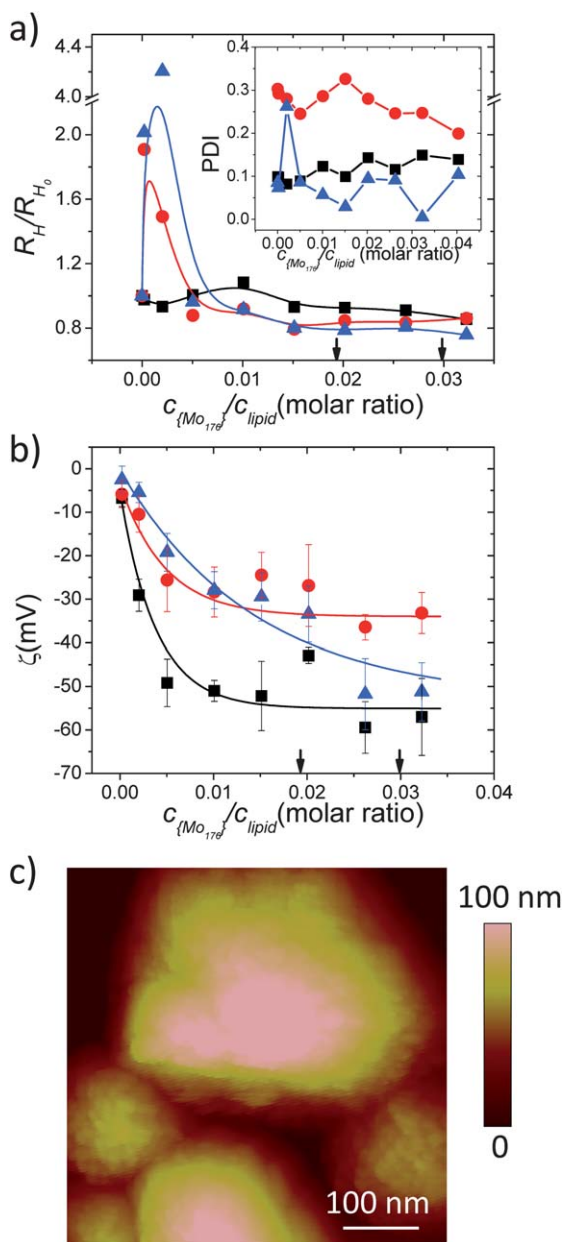


Fig. 4 (a) The ratio of measured DSPC liposome diameter after adding $\{\text{Mo}_{176}\}$ to the original size of bare liposomes against $c_{\{\text{Mo}_{176}\}}/c_{\text{lipid}}$ at $T = 25\text{ }^\circ\text{C}$ (black squares), at which DSPC is in a gel phase, and at $T = 60\text{ }^\circ\text{C}$ (red circles), at which DSPC is in a fluid phase, and cooling back from $T = 60\text{ }^\circ\text{C}$ to $T = 25\text{ }^\circ\text{C}$ (blue triangles). Inset: polydispersity in the $\{\text{Mo}_{176}\}$ -dressed liposome size. (b) Zeta potential, ζ , of DSPC liposomes after adding $\{\text{Mo}_{176}\}$ against $c_{\{\text{Mo}_{176}\}}/c_{\text{lipid}}$ at $T = 25\text{ }^\circ\text{C}$ (black squares), $60\text{ }^\circ\text{C}$ (red circles), and back to $T = 25\text{ }^\circ\text{C}$ (blue triangles). (c) AFM micrograph displays the structure of $\{\text{Mo}_{176}\}$ -dressed DSPC liposomes at $c_{\{\text{Mo}_{176}\}}/c_{\text{lipid}} = 0.027$.

Conclusions

In summary, we have reported that an anionic POM macroion can effectively and firmly bind with zwitterionic or cationic lipids due to strong electrostatic attraction, resulting in a surprising fluid-to-gel phase transition and morphology disruption of the lipid bilayer. To the best of our knowledge, it is



Fig. 5 Schematic illustration of POM-induced phase and morphology instability of lipid bilayer. The light orange lipids are depicted as the lipids in the fluid phase while the dark red lipids are depicted as the ones in the gel phase.

the first time that both phase and morphological instability can be induced by a single POM macroion system, otherwise only one of these is observed with hydrophilic or semi-hydrophobic nanoparticles of $R > 10$ nm, respectively. Direct calorimetric measurements with lipid bilayers of varied lipid chemistry and phase state indicate that the energy release of liposome upon macroion binding is contributed to not only by enthalpy, associated with the gelation of lipid bilayer, but also by entropy, associated with local surface contraction of the lipid bilayer, the latter of which is surprising due to the intuition of the nearly molecular dimensions of the POM macroion being comparable to the size and spacing of the headgroups in the lipid bilayer. Hence, the phenomena reported in this work should be distinguished from the reported structural modification of lipid bilayers by nanoparticles of $R > 10$ nm in colloidal nature. Convincingly, POM macroion-induced surface reconstruction of the lipid bilayer is evident by the observed liposome shrinkage and morphological disruption including the formation of pores, buds, and multilayer stacks on macroion-adsorbed lipid bilayer as schematically illustrated (Fig. 5). These findings promise to provide a model system to quantify the charge interaction between macroion and cell membrane, and give new insight into the design of nanomaterials for controlled drug delivery and minimal cytotoxicity by modulating the thermodynamic properties of cell membranes.

Acknowledgements

We are grateful to the financial support from the US Department of Energy, Office of Basic Sciences, Division of Materials Science and Engineering under grant no. DE-FG02-07ER46390. We thank Dr H. Miras and Dr J. Yan for their assistance in POM synthesis. We are also indebted to Emily Y. Wang for her help with MATLAB programming for the macroion-lipid interaction calculation, Jie Qiu for her help with SAXS, UV-vis spectroscopy experiments, and the Center for Environmental Science and Technology and the Innovation Park at the University of Notre Dame for their instrument supports.

Notes and references

1 N. Murthy, J. R. Robichaud, D. A. Tirrell, P. S. Stayton and A. S. Hoffman, *J. Controlled Release*, 1999, **61**, 137–143.

- 2 J. O. Rädler, I. Koltover, T. Salditt and C. R. Safinya, *Science*, 1997, **275**, 810–814.
- 3 S. El-Andaloussi, T. Holm and U. Langel, *Curr. Pharm. Des.*, 2005, **11**, 3597–3611.
- 4 B. Wang, L. Zhang, S. C. Bae and S. Granick, *Proc. Natl. Acad. Sci. U. S. A.*, 2008, **105**, 18171–18175.
- 5 S. May, D. Harries and A. Ben-Shaul, *Phys. Rev. Lett.*, 2002, **89**, 268102.
- 6 E. C. Mbamala, A. Ben-Shaul and S. May, *Biophys. J.*, 2005, **88**, 1702–1714.
- 7 D. Grillo, M. Olvera de la Cruz and I. Szleifer, *Soft Matter*, 2011, **7**, 4672–4679.
- 8 H. Schiessel, *Eur. Phys. J. B*, 1998, **6**, 373–380.
- 9 M. Schulz, A. Olubummo and W. H. Binder, *Soft Matter*, 2012, **8**, 4849–4864.
- 10 S. Hong, A. U. Bielinska, A. Mecke, B. Keszler, J. L. Beals, X. Shi, L. Balogh, B. G. Orr, J. R. Baker and M. M. Banaszak Holl, *Bioconjugate Chem.*, 2004, **15**, 774–782.
- 11 A. Mecke, S. Uppuluri, T. M. Sassanella, D.-K. Lee, A. Ramamoorthy, J. J. R. Baker, B. G. Orr and M. M. Banaszak Holl, *Chem. Phys. Lipids*, 2004, **132**, 3–14.
- 12 S. Hong, P. R. Leroueil, E. K. Janus, J. L. Peters, M.-M. Kober, M. T. Islam, B. G. Orr, J. R. Baker and M. M. Banaszak Holl, *Bioconjugate Chem.*, 2006, **17**, 728–734.
- 13 D. Hirsch-Lerner and Y. Barenholz, *Biochim. Biophys. Acta, Biomembr.*, 1998, **1370**, 17–30.
- 14 K. A. Brogden, *Nat. Rev. Microbiol.*, 2005, **3**, 238–250.
- 15 K. L. H. Lam, H. Wang, T. A. Siaw, M. R. Chapman, A. J. Waring, J. T. Kindt and K. Y. C. Lee, *Biochim. Biophys. Acta, Biomembr.*, 2012, **1818**, 194–204.
- 16 A. G. Lee, *Biochim. Biophys. Acta, Biomembr.*, 2003, **1612**, 1–40.
- 17 S. H. White and W. C. Wimley, *Annu. Rev. Biophys. Biomol. Struct.*, 1999, **28**, 319–365.
- 18 A. Dolbecq, E. Dumas, C. d. R. Mayer and P. Mialane, *Chem. Rev.*, 2010, **110**, 6009–6048.
- 19 T. Douglas and M. Young, *Nature*, 1998, **393**, 152–155.
- 20 D.-L. Long, E. Burkholder and L. Cronin, *Chem. Soc. Rev.*, 2007, **36**, 105–121.
- 21 A. Müller, H. Reuter and S. Dillinger, *Angew. Chem., Int. Ed.*, 1995, **34**, 2328–2361.
- 22 T. Liu, E. Diemann, H. Li, A. W. M. Dress and A. Müller, *Nature*, 2003, **426**, 59–62.
- 23 G. J. T. Cooper and L. Cronin, *J. Am. Chem. Soc.*, 2009, **131**, 8368–8369.
- 24 J. Zhang, Y.-F. Song, L. Cronin and T. Liu, *J. Am. Chem. Soc.*, 2008, **130**, 14408–14409.
- 25 T. Liu, M. L. K. Langston, D. Li, J. M. Pigga, C. Pichon, A. M. Todea and A. Müller, *Science*, 2011, **331**, 1590–1592.
- 26 R. Neumann, *Prog. Inorg. Chem.*, 1998, **47**, 317–370.
- 27 C. L. Hill and C. M. Prosser-McCarthy, *Coord. Chem. Rev.*, 1995, **143**, 407–455.
- 28 J. Lehmann, A. Gaita-Arino, E. Coronado and D. Loss, *Nat. Nanotechnol.*, 2007, **2**, 312–317.
- 29 J. T. Rhule, C. L. Hill, D. A. Judd and R. F. Schinazi, *Chem. Rev.*, 1998, **98**, 327–358.
- 30 M. T. Pope and A. Müller, *Angew. Chem., Int. Ed.*, 1991, **30**, 34–48.

- 31 B. Hasenknopf, *Front. Biosci.*, 2005, **10**, 275–287.
- 32 C. L. Hill, M. S. Weeks and R. F. Schinazi, *J. Med. Chem.*, 1990, **33**, 2767–2772.
- 33 T. Liu, *Langmuir*, 2010, **26**, 9202–9213.
- 34 R. Carr, I. A. Weinstock, A. Sivaprasadarao, A. Müller and A. Aksimentiev, *Nano Lett.*, 2008, **8**, 3916–3921.
- 35 A. Müller, A. Merca, A. J. M. Al-Karawi, S. Garai, H. Bögge, G. Hou, L. Wu, E. T. K. Haupt, D. Rehder, F. Haso and T. Liu, *Chem.–Eur. J.*, 2012, **18**, 16310–16318.
- 36 A. Müller, E. Krickemeyer, H. Bögge, M. Schmidtman, C. Beugholt, P. Kögerler and C. Z. Lu, *Angew. Chem., Int. Ed.*, 1998, **37**, 1220–1223.
- 37 G. S. Manning, *J. Chem. Phys.*, 1969, **51**, 924–933.
- 38 H. P. Simonian, L. Vo, S. Doma, R. S. Fisher and H. P. Parkman, *Dig. Dis. Sci.*, 2005, **50**, 2276–2285.
- 39 A. Velázquez-Campoy, H. Ohtaka, A. Nezami, S. Muzammil and E. Freire, in *Current Protocols in Cell Biology*, John Wiley & Sons, Inc., 2001.
- 40 B. Jing and Y. Zhu, *J. Am. Chem. Soc.*, 2011, **133**, 10983–10989.
- 41 J. P. Prates Ramalho, P. Gkeka and L. Sarkisov, *Langmuir*, 2011, **27**, 3723–3730.
- 42 M. R. Rasch, E. Rossinyol, J. L. Hueso, B. W. Goodfellow, J. Arbiol and B. A. Korgel, *Nano Lett.*, 2010, **10**, 3733–3739.
- 43 http://www.physics.oregonstate.edu/portfolios/Activities/EM_Activities/ElectricPotentialRing/RingVSolutions070701.pdf.
- 44 http://avantilipids.com/index.php?option=com_content&view=article&id=260&Itemid=212&catnumber=840051.
- 45 M. L. Kistler, K. G. Patel and T. Liu, *Langmuir*, 2009, **25**, 7328–7334.
- 46 S.-i. Noro, R. Tsunashima, Y. Kamiya, K. Uemura, H. Kita, L. Cronin, T. Akutagawa and T. Nakamura, *Angew. Chem., Int. Ed.*, 2009, **48**, 8703–8706.
- 47 <http://www.uic.edu/classes/phys/phys450/MARKO/N016.html>.
- 48 J. C. Mathai, S. Tristram-Nagle, J. F. Nagle and M. L. Zeidel, *J. Gen. Physiol.*, 2007, **131**, 69–76.
- 49 B. P. Gaber and J. P. Sheridan, *Biochim. Biophys. Acta, Biomembr.*, 1982, **685**, 87–93.
- 50 R. A. Parente, M. Höchli and B. R. Lentz, *Biochim. Biophys. Acta, Biomembr.*, 1985, **812**, 493–502.
- 51 J. Hernandez-Borrell and K. M. W. Keough, *Biochim. Biophys. Acta, Biomembr.*, 1993, **1153**, 277–282.
- 52 E. B. Smaal, K. Nicolay, J. G. Mandersloot, J. de Gier and B. de Kruijff, *Biochim. Biophys. Acta, Biomembr.*, 1987, **897**, 453–466.
- 53 J. F. Nagle and S. Tristram-Nagle, *Biochim. Biophys. Acta, Rev. Biomembr.*, 2000, **1469**, 159–195.